

02,05

## Interaction modes of magnetized HTSC tapes stacks

© A.I. Podlivaev<sup>1,2</sup>, I.A. Rudnev<sup>1</sup>

<sup>1</sup> National Research Nuclear University „MEPhI“,  
Moscow, Russia

<sup>2</sup> Research Institute of Problems in the Development of Scientific and Educational Potential of Young People,  
Moscow, Russia

E-mail: AIPodlivayev@mephi.ru

Received September 16, 2021

Revised September 16, 2021

Accepted October 11, 2021

On the basis of the critical state model, the interaction force of a pair of magnetic lines, which are sets of magnetized stacks of second-generation HTSC tapes, is calculated. The modes of magnetization of interacting rulers by an external magnetic field and the origin of the magnetization reversal of the stacks of tapes during multiple cycles of approaching — moving the rulers away from each other are considered. The force of interaction of the rulers is determined depending on the distance between them and the number of the cycle.

**Keywords:** high-temperature superconductors, second-generation HTSC tapes, magnetic levitation, force of interaction, critical state

DOI: 10.21883/PSS.2022.02.54004.205

### 1. Introduction

Sources of a spatially nonuniform magnetic field are being improved constantly, since they have various engineering applications (see, e.g., the review in [1] and references therein and papers [2–8]). A combination of magnets producing a nonuniform magnetic field [2–8] is one of the basic elements of various contactless magnetic-levitation devices (transport, frictionless bearings, etc.). Sources of magnetic fields with high flux densities and significant field gradients are needed to construct magnetic-levitation systems. The gradient configuration of a magnetic field is often produced by a set of heteropolar permanent magnets. The remanent flux density of modern permanent magnets, which is within 0.5 T for commonly used NdFeB magnets, is one of the factors limiting the applicability of this approach. A stronger constant field with its gradient remaining high may be produced with the use of trapped-flux magnets based on superconductors. Magnetized in a strong magnetic field, such structures are capable of trapping and storing immensely intense magnetic fields. Specifically, bulk HTSCs can trap magnetic fields of 17.6 T at low temperatures [9,10], while stacks of HTSC tapes trap fields of 17.7 T [11]. The remanent magnetization of HTSCs is associated with the pinning effect. Magnetized HTSCs trap the magnetic flux in the form of Abrikosov vortices and have the capacity to maintain a high magnetic flux density (exceeding the one of permanent magnets) for a long time on their surfaces [9–11]. An HTSC field source has an advantage in this capacity to produce a high-intensity magnetic field, but it also has several drawbacks. Specifically, an insufficiently cooled magnetized superconductor is prone to thermodynamic instability [12,13] that may result in loss of the remanent magnetic moment. In

addition, the remanent HTSC magnetization in systems based on it may degrade both with time (due to flux creep) [14] and under the influence of external variable magnetic fields [15]. However, the use of superconducting magnets is undeniably advantageous due to a manifold increase in the field magnitude. A comparative analysis of the efficiency of levitation systems with a nonuniform magnetic field produced by permanent NdFeB magnets and stacks of GdBaCuO HTSC tapes was performed in [16]. It was demonstrated that the use of superconductors is advantageous in terms of the lift force of levitation systems with a gradient magnetic field source if the characteristic size of a field nonuniformity is greater than 38 mm at liquid nitrogen temperature (or 6 mm at liquid neon temperature). If the field nonuniformity is smaller in size, systems based on permanent magnets are more efficient. The present study is also focused on a system where a permanent magnet is replaced by a magnetized stack of HTSC tapes. At the same time, the effects of remagnetization of superconductors may introduce certain corrections relevant to further use of trapped-flux magnets in real-life levitation systems. The processes of remagnetization of the gradient magnetic field source were not examined in [16] (this approximation is valid if the interaction between different parts of a levitation system is relatively weak). The present paper is the first to consider the general case (i.e., investigate the processes of remagnetization of superconducting parts of a magnetic levitation suspension under cyclic load).

We study nonuniform configurations of currents of HTSC tapes that comprise the levitation system. Nonuniform states of magnetic tapes of various types are examined within different approaches in accordance with the scale of nonuniformity. The density-functional theory calculation method may be used at the atomic level [17]. The

nonuniformity due to the microscopic grain structure may induce uncommon physical effects such as the emergence of phase transitions in current (similar to those observed in granular  $\text{YBa}_2\text{Cu}_3\text{O}_{7-x}$  superconductors [18]). The influence of granulation of the HTSC structure on the hysteretic nature of magnetoresistance was demonstrated experimentally in [19,20]. The size range of nonuniformities typical of levitation applications lies above several millimeters. This is the characteristic size of nonuniformities of the magnetic field and currents that is examined in the present study.

## 2. Problem formulation

Let us consider a system comprising two parallel stacks of HTSC tapes (i.e., a magnetic suspension). The projection of the HTSC suspension on plane  $(X, Z)$  is shown in Fig. 1. The upper part of the superconducting suspension is fixed, while the lower part moves in the vertical direction with coordinate  $Z(t)$ , where  $t$  is time. At the initial time  $t = 0$ , both parts are unmagnetized. External magnetic field  $\mathbf{B}_{\text{ext}}(t)$ , which is spatially uniform and varies in time, is used to magnetize both parts of the suspension. The only nonzero normal component of this field is  $B_Z(t) = B_{\text{max}}t$  at  $0 \leq t \leq t_0$ ,  $B_Z(t) = B_{\text{max}}(2 - t)$  at  $t_0 \leq t \leq 2t_0$ , and  $B_Z(t) = 0$  at  $2t_0 \leq t$ . Just as in [16,21,22], an HTSC tape with superconducting GdBaCuO on a substrate made of a nickel-chrome-molybdenum alloy with protective layers of copper and silver was used as the superconducting base. The total thickness of the HTSC tape is 0.1 mm, and superconducting layer thickness  $d = 1.5 \mu\text{m}$ . The HTSC tape width is  $a = 12 \text{ mm}$ . Magnetization is performed adiabatically slowly; i.e., the value of characteristic magnetization time  $t_0$  is chosen so that the residual currents induced in superconducting stacks are independent of it. Magnitude  $B_{\text{max}}$  needed to achieve the maximum magnetization of the sample depended on number  $N_l$  of individual tapes in the stack. Two values of  $N_l = 1$  and 20 and the corresponding  $B_{\text{max}} = 1$  and 5 T were chosen for calculations. The maximum value of  $N_l = 20$  was chosen based on the data from [16], where the need to limit the thickness of stacks of HTSC tapes for levitation applications was demonstrated. It does indeed follow from the results of [16] that the magnetic field above a periodic HTSC line with a thickness equal to half a period (6 mm for tapes with a width of 12 mm) is almost the same as the magnetic field of an HTSC stack of an infinite thickness. Following this line of reasoning, we limited ourselves to comparing stacks containing 1 and 20 tapes (the corresponding stack thicknesses are 0.1 and 2 mm). A further increase in the stack height was assumed to be inefficient. The following form of time dependence  $Z(t)$  of the distance between the upper and the lower suspension parts was chosen:  $Z(t) = a$  at  $0 \leq t \leq 2t_0$  and  $Z(t) = a[1 + q + (1 - q) \cos(2\pi(t/t_0 - 2))]/2$  at  $2t_0 \leq t$ . This form of dependence  $Z(t)$  appears to be the simplest and the most fitting in the case when both the initial

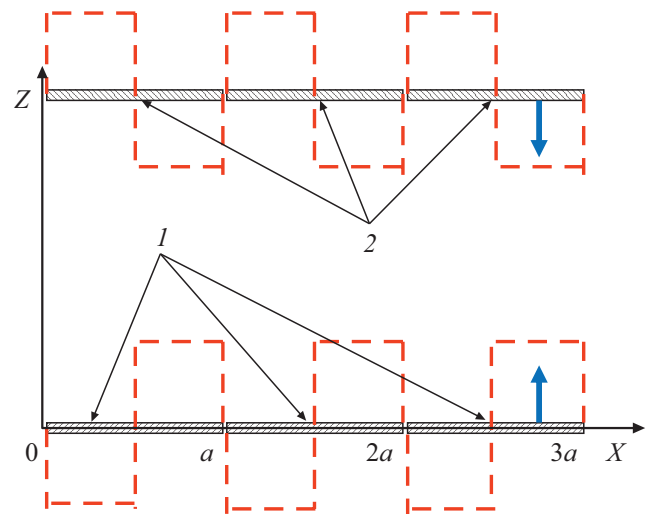


**Figure 1.** Structure of the magnetic suspension. 1 and 2 are the stacks of HTSC tapes of the upper and the lower suspension parts, respectively. Each stack is isolated from the neighboring one, has width  $a$ , and consists of  $N_l$  individual tapes positioned one above the other in the  $Z$  direction. The length of the stack in the direction of axis  $Y$  is assumed to be Indefinite. The structure is assumed to be periodic in the direction of axis  $X$  (the period is  $a$ ). Current density  $j_y$  induced by an external magnetic field in the upper and the lower suspension parts is represented schematically by the dashed line. Bold arrows on the right denote the directions of magnetization of stacks of the upper and the lower suspension parts.

magnetization and subsequent oscillations need to be characterized simultaneously. Parameter  $q$  defines the amplitude of oscillations and sets the distance of closest approach for the layers. The interplanar distance remains unchanged within the first time interval  $t \leq 2t_0$  that corresponds to the magnetization stage. The external field is nonzero within this interval. When it comes to an end, the field becomes zero and the interplanar distance starts oscillating. The values of  $q = 0.1, 0.05$ , and  $0.02$  were used in subsequent calculations. The oscillatory nature of variation of the distance between the upper and the lower suspension parts allows one to examine the transient processes of suspension operation under variable vertical loads and determine the steady-state mode under such oscillations of height  $Z(t)$ .

The induction, Biot–Savart [23], and Ohm’s laws, which govern supercurrents, are written as

$$\frac{\partial \mathbf{B}}{\partial t} = -\nabla \times \mathbf{E},$$

$$\mathbf{B}(\mathbf{R}) = \mathbf{B}_{\text{ext}}(t) + \frac{\mu_0}{4\pi} \int_S \frac{\mathbf{j}(\mathbf{r}) \times (\mathbf{R} - \mathbf{r})}{|\mathbf{R} - \mathbf{r}|^3} d^3r, \quad \mathbf{E} = \rho(|\mathbf{j}|)\mathbf{j}. \quad (1)$$

Symbols  $\mathbf{B}$ ,  $\mathbf{E}$ , and  $\mathbf{j}$  denote the magnetic-field vector, the electric-field vector, and the vector density of induced supercurrents, respectively.  $S$  is the region of supercurrents, and  $\mu_0$  and  $\rho(|\mathbf{j}|)$  are the magnetic constant and the

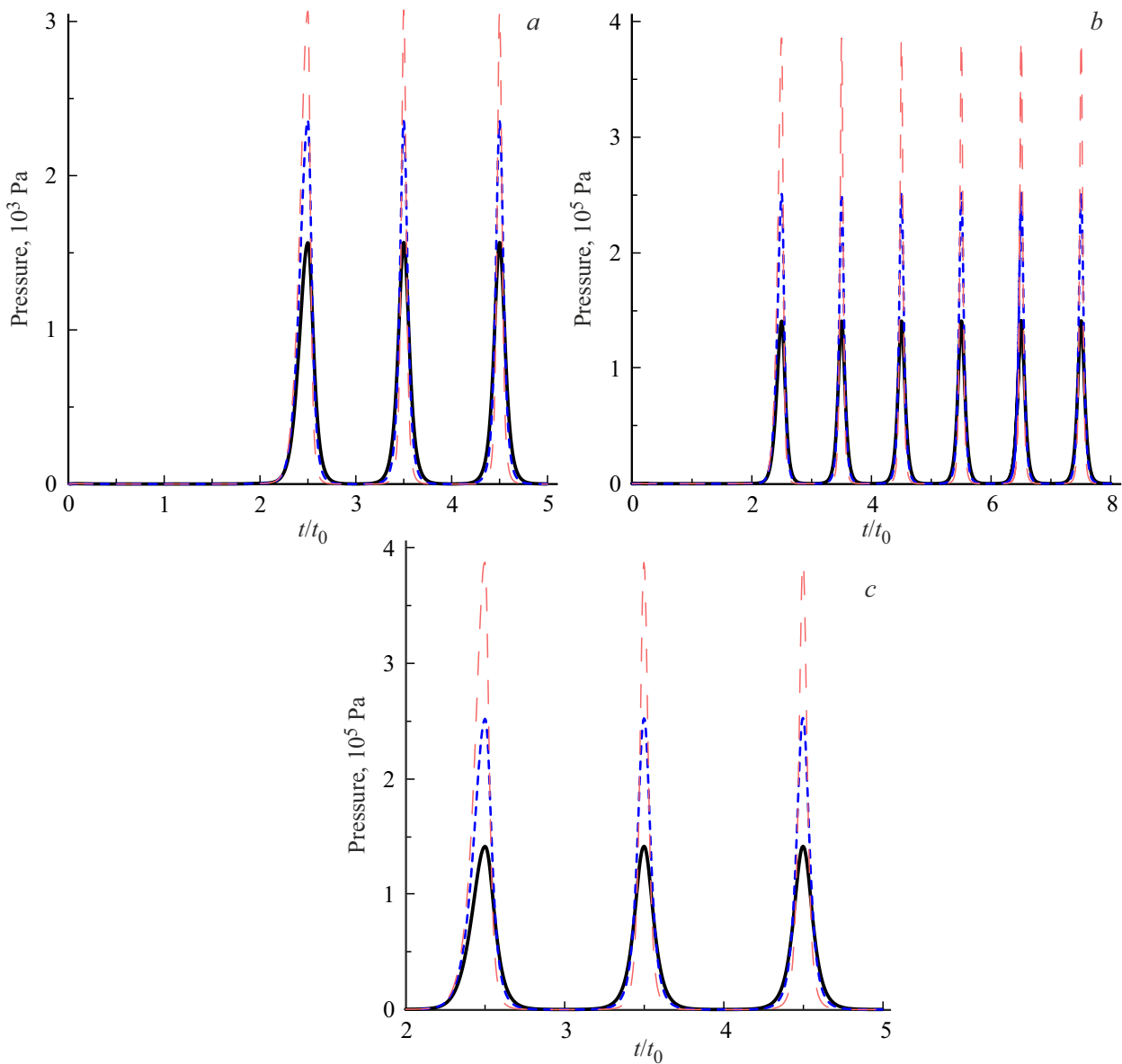


**Figure 2.** Time dependence of the pressure exerted by the upper magnetic suspension part on the lower one. The magnetization stage and the first three periods of approach of the upper part to the lower one,  $N_l = 1$  (a). The magnetization stage and the first six periods of approach of the upper part to the lower one,  $N_l = 20$  (b). The first three periods,  $N_l = 20$  (c). Bold solid curve:  $q = 0.1$ ; dashed curve:  $q = 0.05$ ; thin dashed curve:  $q = 0.02$ .

specific resistance of the superconductor that was defined, following [16,22], as

$$\rho(\mathbf{j}, B) = \begin{cases} 0, & |\mathbf{j}| < j_c(B), \\ \rho_0[|\mathbf{j}| - j_c(B)]^2, & j_c(B) \leq |\mathbf{j}|, \end{cases}$$

$$j_c(B) = A_1 \exp(-|B|/\beta_1) + A_2 \exp(-|B|/\beta_2). \quad (2)$$

The following values correspond to the volumetric critical density of supercurrent in GdBaCuO at liquid nitrogen temperature:  $A_1 = 2.3665 \cdot 10^8 \text{ A/m}^2$ ,  $A_2 = 1.7884 \cdot 10^8 \text{ A/m}^2$ ,  $\beta_1 = 0.1175 \text{ T}$ , and  $\beta_2 = 1.2238 \text{ T}$  [18]. A detailed description of Eqs. (1), (2) and an algorithm for solving the above problem numerically were presented in [24]. In view of

their cumbersomeness, they are not discussed here. Two-dimensional density of supercurrents  $J$  is expressed in A/m and is related to volumetric density  $j$  in the following way:  $J = j d$ . The Ampère’s circuital law defined the force with which the field density of the lower suspension part acted on supercurrents in the upper part.

### 3. Results

Figure 2 presents the time dependence of the force of interaction between two suspension parts normalized to a unit surface for the suspension formed by HTSC tape stacks with  $N_l = 1$  and 20. With the chosen  $Z(t)$

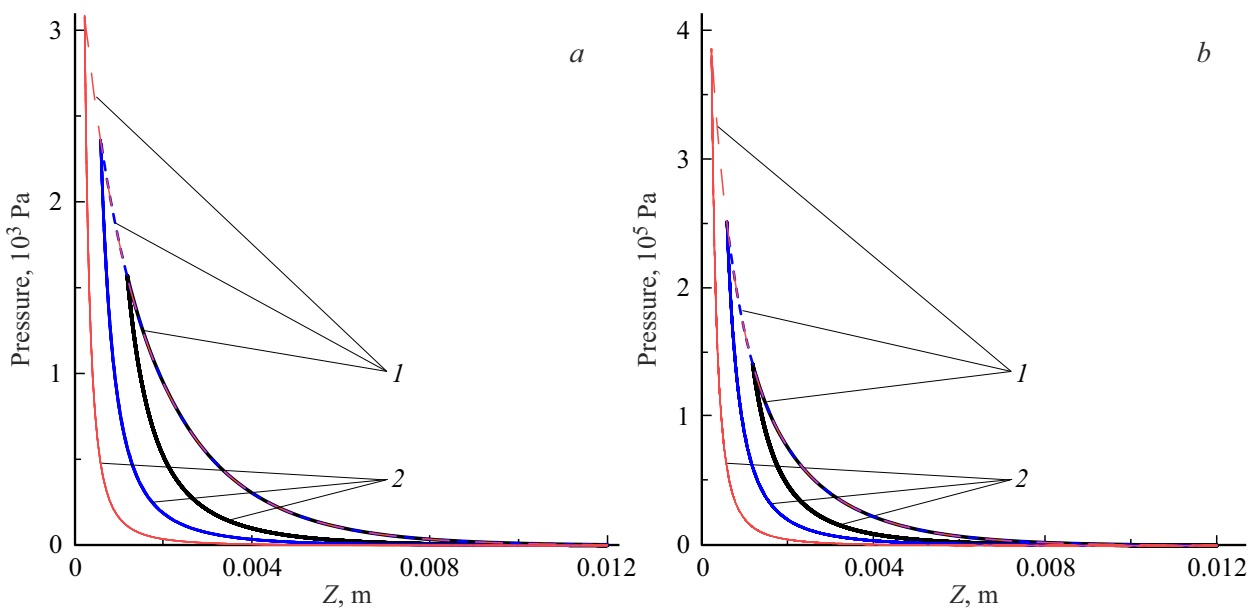


**Figure 3.** Dependence of the pressure exerted on the lower magnetic suspension part by the upper one on the distance between them. The number of tapes in a stack is  $N_l = 1$  (a),  $N_l = 20$  (b). Six periods of approach of the upper part to the lower one are presented. Bold solid curve:  $q = 0.1$ ; dashed curve of an average thickness:  $q = 0.05$ ; thin dashed curve:  $q = 0.02$ . 1 — sections of the dependence corresponding to time interval  $2 \leq t/t_0 \leq 2.5$  (the first approach of the upper suspension part to the lower one); 2 — sections of the dependence corresponding to time interval  $2.5 \leq t/t_0 \leq 8$  (steady-state oscillation mode).

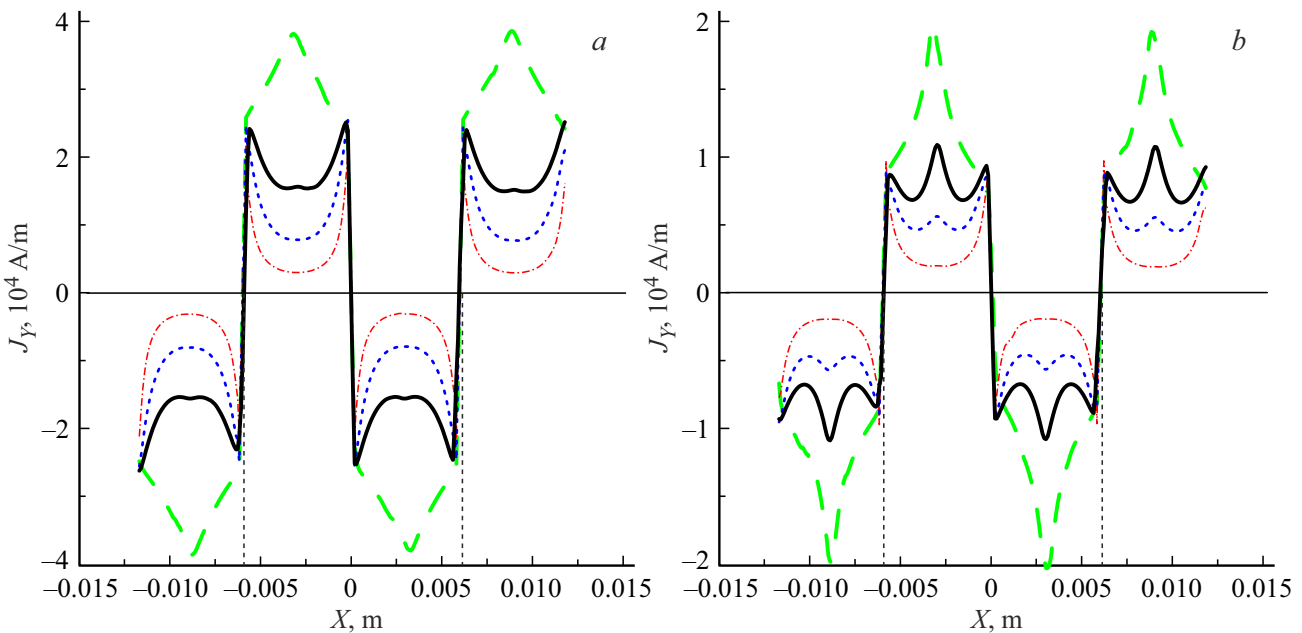


**Figure 4.** Two-dimensional current density  $J_Y(X)$  (A/m) in the lower part of the suspension consisting of a single ( $N_l = 1$ ) tape (a) and average two-dimensional current density  $J_Y(X)$  per a single tape in a stack of 20 tapes ( $N_l = 20$ ) (b). Bold dashed curve: density after magnetization before the first approach of the upper suspension part to the lower one ( $t/t_0 = 2$ ). Bold solid curve:  $q = 0.1$ ; dashed curve:  $q = 0.05$ ; dash-and-dot curve:  $q = 0.02$  at the end time point  $t/t_0 = 8$  after six oscillations. Thin vertical dashed lines denote the boundaries of tape stacks.

dependence, the maximum distance between the suspension parts is 12 mm. The value of  $Z(t)$  is maximized at  $0 \leq t/t_0 \leq 2$  and at  $t/t_0 = 3, 4, 5, \dots$ . It can be seen from Fig. 2 that the magnetic interaction is almost zero at the

maximum separation. The force of repulsion between the two parts reaches its maximum when the  $Z(t)$  distance is minimized at time points  $t/t_0 = 2.5, 3.5, 4.5, 5.5, \dots$ . The large-scale plot for  $N_l = 20$  in Fig. 2, c demonstrates that

the first peak (for all values of  $q$ ) differs in shape from the subsequent peaks, which are all congruent. Figure 3 presents the time dependence of the force of interaction between two suspension parts within time interval  $2 \leq t/t_0 \leq 8$  on the distance between them. It is evident that the curves within time interval  $2 \leq t/t_0 \leq 2.5$  (these sections are denoted with number 1 in Fig. 3) in each type of suspension differ in shape from the curves within  $2.5 \leq t/t_0 \leq 8$  (denoted with number 2) where the motion is strictly periodic. The trajectory of periodic motion of a one-dimensional body with friction plotted in force–displacement coordinates assumes the shape of a hysteretic curve. The area under this curve is equal to the energy dissipated due to friction forces within a single cycle. Judging by the shape of curves in Fig. 3, energy dissipation is observed only within the  $2 \leq t/t_0 \leq 2.5$  interval. This dissipation is attributable to the release of energy associated with the detachment of the system of Abrikosov vortices from HTSC pinning centers. Hysteresis is not observed within the  $2.5 \leq t/t_0 \leq 8$  interval; i.e., energy dissipation is lacking, and the magnetic suspension is an ideal nonlinear spring. The stiffness of this spring depends on the oscillation amplitude and increases significantly as the suspension parts move closer to each other. The mutual pressure of suspension parts also increases in this case and may reach 3100 Pa for the single-layer suspension, while the peak repulsive pressure in the multilayer suspension ( $N_l = 20$ ) is 400000 Pa ( $\sim 4$  atmospheres). If the critical current was not suppressed by the magnetic field (see expression (2)), the dependence of the peak repulsive pressure would be strictly quadratic, since this quantity depends on the product of current densities of one suspension part and the normal component of the magnetic field produced by the other part. The ratio of forces in the multilayer and single-layer suspensions would then be equal to  $(N_l)^2 = 400$ . The suppression of the critical current by the magnetic field reduces this ratio to  $400000/3100 = 129$ . The mutual influence of currents of two suspension parts via the magnetic field is illustrated in Fig. 4 that presents the distributions of two-dimensional supercurrent density  $J_Y(X)$  after magnetization (but before the first approach of one suspension part to the other one) and after subjecting the suspension parts to six approach–recession cycles. It follows from the comparison of Figs. 4, *a, b* that the density of currents in each individual tape of the multilayer stack ( $N_l = 20$ ) is significantly lower than the corresponding value in the single-layer stack (as was expected, the current density is maximized at  $X = \pm a/2$ , and its maximum value is  $\sim 40000$  F/m in the single-layer suspension and as high as  $\sim 20000$  A/m in the multilayer suspension). The process of demagnetization is, in general, more extensive in the single-layer stack. This is evidenced, e.g., by the fact that the central peak of current density (at  $X = \pm a/2$ , Fig. 4, *b*) is preserved well in the multilayer stack after oscillations with parameter  $q = 0.1$ , while the same peak in the single-layer stack vanishes almost completely. Prior to the onset of oscillations, the critical current density

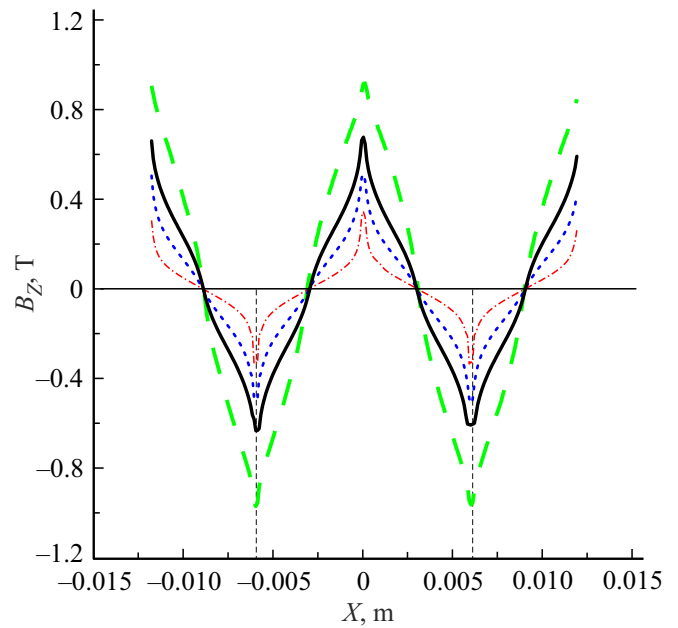


**Figure 5.** Normal component of the field density above the suspension surface in case of the maximum separation between the suspension parts. Bold dashed curve: distribution after magnetization before the first approach of the upper suspension part to the lower one ( $t/t_0 = 2$ ). Bold solid curve:  $q = 0.1$ ; dashed curve:  $q = 0.05$ ; dash-and-dot curve:  $q = 0.02$  at the end time point  $t/t_0 = 8$  after six oscillations.

decreases most significantly near the tape edges where the internal magnetic field of the stack is maximized (see Fig. 5 that presents the dependence of normal component  $B_z(X)$  of the field density on the multilayer suspension surface in case of the maximum separation between the upper and the lower suspension parts). Figure 5 also shows that the peak field density values are significantly higher than the value of  $\beta_1 = 0.1175$  T, which characterizes the suppression of the critical current density by the magnetic field in two-exponential approximation (2), even in case of the maximum demagnetization ( $q = 0.02$ , dash-and-dot curve). This is the reason why the supercurrent density is highly nonuniform in both parts of the suspension.

## 4. Conclusion

A fundamentally new design of a levitation suspension based on stacks of superconducting tapes made without the use of traditional ferromagnetic materials was presented. Theoretical calculations revealed the existence of viable conservative suspension operation modes with no energy dissipation, which is invariably accompanied by heating of superconductors, in the proposed system. In the case of multiple oscillations, the conservative mode was found to be established within a single oscillation (the first one). It was demonstrated that the lift force of the suspension increases by a factor of  $\sim 130$  as the number of tapes

in superconducting parts of the suspension varies from 1 to 20. If the number of tapes increases further, no significant changes in the lift force are observed, since the supercurrent in suspension parts is suppressed by the internal magnetic field. The obtained theoretical data have a certain predictive power: the distribution of the magnetic field on the surface of suspension parts may be measured experimentally using the methods of Hall magnetometry. It is also not without interest to determine the change in levitation force and the power dissipation occurring when suspension parts are displaced transversely relative to each other.

### Funding

This study was supported financially by the Russian Science Foundation (project No. 17-19-01527).

### Conflict of interest

The authors declare that they have no conflict of interest.

### References

- [1] F. Balci, A. Bingolbali, N. Dogan, M. Irfan. *Tech. Phys. Lett.* **47**, 4, 3 (2021).
- [2] I. Valiente-Blanco, E. Diez-Jimenez, C. Cristache, M.A. Alvarez-Valenzuela, J.L. Perez-Diaz. *Tribology Lett.* **6** (2013). DOI: 10.1007/s11249-013-0204-0
- [3] F. Antoncik, M. Lojka, T. Hlasek, V. Bartunek, I. Valiente-Blanco, J.L. Perez-Diaz, O. Jankovsky. *Supercond. Sci. Technol.* **33**, 045010 (2020). <https://doi.org/10.1088/1361-6668/ab6e8e>
- [4] M. Osipov, I. Anishenko, A. Starikovskii, D. Abin, S. Pokrovskii, A. Podlivaev, I. Rudnev. *Supercond. Sci. Technol.* **34**, 035033 (2021). DOI.org/10.1088/1361-6668/abda5a
- [5] J.G. Storey, M. Szmigie, F. Robinson, S.C. Wimbush, R.A. Badcock. *IEEE Transact. Appl. Supercond.* **30**, 4, 600706 (2020). DOI: 10.1109/TASC.2020.2982884.
- [6] Y. Miyazaki, K. Mizuno, T. Yamashita, M. Ogata, H. Hasegawa, K. Nagashima, S. Mukoyama, T. Matsuoka, K. Nakao, S. Horiuchi, T. Maeda, H. Shimizu. *Cryogenics* **80**, 234 (2016).
- [7] P. Bernstein, J. Noudem. *Supercond. Sci. Technol.* **33**, 3, 033001 (2020). DOI: 10.1088/1361-6668/ab63bd
- [8] Kun Liu, Wenjiao Yang, Guangtong Ma, Loïc Quéval, Tianyong Gong, Changqing Ye, Xiang Li, Zhen Luo. *Supercond. Sci. Technol.* **31**, 015013 (2018). [doi.org/10.1088/1361-6668/aa987b](https://doi.org/10.1088/1361-6668/aa987b)
- [9] M. Tomita, M. Murakami. *Nature* **421**, 517 (2003).
- [10] J.H. Durrell, A.R. Dennis, J. Jaroszynski, M.D. Ainslie, K.G.B. Palmer, Y-H. Shi, A.M. Campbell, J. Hull, M. Strasik, E.E. Hellstrom. *Supercond. Sci. Technol.* **27**, 8, 082001 (2014).
- [11] A. Patel, A. Baskys, T. Mitchell-Williams, A. McCaul, W. Coniglio, J. Hänisch, B.A. Glowacki. *Supercond. Sci. Technol.* **31**, 09LT01 (2018).
- [12] V.R. Romanovskii. *Tech. Phys.* **62**, 1, 58 (2017). DOI: 10.21883/JTF.2017.01.44018.1823
- [13] V.R. Romanovskii. *Tech. Phys.* **62**, 4, 560 (2017). DOI: 10.21883/JTF.2017.04.44313.1943x90
- [14] D. Abin, M. Osipov, S. Pokrovskii, I. Rudnev. *IEEE Trans. Appl. Supercond.* **26**, 3, 8800504 (2016). DOI: 10.1109/TASC.2016.2525924.
- [15] S. Pokrovskii, A. Dmitry, M. Osipov, I. Rudnev. *IEEE Trans. Appl. Supercond.* **26**, 3, 8201304 (2016). DOI: 10.1109/TASC.2016.2533573.
- [16] A.I. Podlivaev, I.A. Rudnev. *Phys. Solid State* **63**, 12, 1757 (2021).
- [17] T.P. Yadav, A. Srivastava, G.C. Kaphle. *Phys. Solid State* **63**, 2, 249 (2021).
- [18] V.V. Derevyanko, T.V. Sukhareva, V.A. Finkel'. *Phys. Solid State* **60**, 3, 470 (2018).
- [19] S.V. Semenov, D.A. Balaev, M.I. Petrov. *Phys. Solid State* **63**, 7, 1069 (2021).
- [20] S.V. Semenov, D.A. Balaev. *Phys. Solid State* **62**, 7, 1136 (2020).
- [21] S.V. Samoilenkov, V.I. Shcherbakov, D.R. Kumarov, D.A. Gorbunova. *Tech. Phys. Lett.* **46**, 1, 23 (2020). DOI: 10.21883/PJTF.2020.01.48860.18047
- [22] A.I. Podlivaev, I.A. Rudnev. *Phys. Solid State* **63**, 6, 888 (2021).
- [23] L.D. Landau, E.M. Lifshitz. *Teoriya polya*. Nauka, M. (1988). 512 pp (in Russian).
- [24] A.I. Podlivaev, I.A. Rudnev. *Supercond. Sci. Technol.* **30**, 035021 (2017). DOI: 10.1088/1361-6668/aa55aa